Acta Crystallographica Section F
Structural Biology and Crystallization Communications
ISSN 1744-3091

The novel 2Fe–2S outer mitochondrial protein mitoNEET displays conformational flexibility in its N-terminal cytoplasmic tethering domain

Andrea R. Conlan,[a] Mark L. Paddock,[b] Herbert L. Axelrod,[c] Aina E. Cohen,[c] Edward C. Abresch,[b] Sandra Wiley,[d] Melinda Roy,[a] Rachel Nechushtai[e] and Patricia A. Jennings[a]*

[a]Departments of Chemistry and Biochemistry, University of California, San Diego, La Jolla, CA 92093, USA, [b]Department of Physics, University of California, San Diego, La Jolla, CA 92093, USA, [c]Department of Pharmacology, University of California, San Diego, La Jolla, CA 92093, USA, [d]Stanford Synchrotron Radiation Laboratory, 2575 Sand Hill Road, Menlo Park, CA 94025, USA, and [e]Department of Plant and Environmental Sciences, The Wolfson Centre for Applied Structural Biology, The Hebrew University of Jerusalem, Jerusalem 91904, Israel

Correspondence e-mail: pajennin@ucsd.edu

Received 6 March 2009
Accepted 22 May 2009

PDB Reference: mitoNEET, 3ew0, re3w0sf.

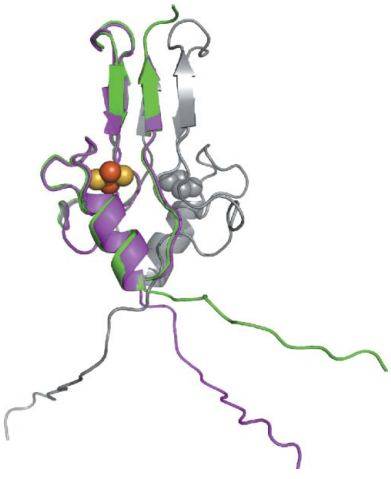

A primary role for mitochondrial dysfunction is indicated in the pathogenesis of insulin resistance. A widely used drug for the treatment of type 2 diabetes is pioglitazone, a member of the thiazolidinedione class of molecules. MitoNEET, a 2Fe–2S outer mitochondrial membrane protein, binds pioglitazone [Colca *et al.* (2004), *Am. J. Physiol. Endocrinol. Metab.* **286**, E252–E260]. The soluble domain of the human mitoNEET protein has been expressed C-terminal to the superfolder green fluorescent protein and the mitoNEET protein has been isolated. Comparison of the crystal structure of mitoNEET isolated from cleavage of the fusion protein (1.4 Å resolution, R factor = 20.2%) with other solved structures shows that the CDGSH domains are superimposable, indicating proper assembly of mitoNEET. Furthermore, there is considerable flexibility in the position of the cytoplasmic tethering arms, resulting in two different conformations in the crystal structure. This flexibility affords multiple orientations on the outer mitochondrial membrane.

1. Introduction

Mitochondrial dysfunction is implicated in the development of type 2 diabetes, with an underlying problem of insulin sensitivity (Lowell & Shulman, 2005). The origin of the chronic malfunction may lie in the diminished oxidative capacity of the mitochondrial electron-transport chains in insulin-sensitive tissue. Pioglitazone, a therapeutic agent for the treatment of type 2 diabetes, is known to enhance oxidative capacity by stimulating mitochondrial biogenesis (Skov *et al.*, 2008). MitoNEET, the protein product of the *CISD1* gene, localizes to the outer mitochondrial membrane (Wiley, Murphy *et al.*, 2007) and was originally identified upon cross-linking to pioglitazone (Colca *et al.*, 2004). The cytoplasmic CDGSH domain of mitoNEET (residues 33–108) contains a novel redox-active 2Fe–2S cluster (Wiley, Paddock *et al.*, 2007) with a novel protein fold (Paddock *et al.*, 2007). Among the unique structural features is that two mitoNEET protomers intertwine to form the newly named 'NEET' fold (Paddock *et al.*, 2007), which consists of two domains, a β-cap and a 2Fe–2S cluster-binding domain (Paddock *et al.*, 2007; Hou *et al.*, 2007; Lin *et al.*, 2007) that includes 3Cys–1His coordination atypical of 2Fe–2S proteins (Meyer, 2008).

Thus, mitoNEET represents a new structural class of Fe–S proteins whose function, while implicated in diabetes, is not completely understood. In order to characterize the protein, many studies with mutations and with its less stable homologs will be necessary. In addition to X-ray crystallographic methods, we are also employing NMR techniques as a complementary method to elucidate structural information on protein–drug interactions and functional information. Two-dimensional homonuclear NMR studies (Paddock *et al.*, 2007) indicate that the overall structure of the protein remains intact upon drug (pioglitazone) binding. However, consistent with the hydrophobic nature of pioglitazone, chemical shift changes in the aromatic and aliphatic resonances as well as stabilization of the amide protons of the Trp75 and Tyr71 residues towards hydrogen/deuterium exchange were observed upon drug binding.

Since at this point neither the mode of pioglitazone binding to mitoNEET nor the mechanism of the stabilization of the Fe–S cluster of mitoNEET by pioglitazone binding have been elucidated, continued structure–function studies are needed, particularly using the well established methods of NMR spectroscopy and X-ray crystallography (Juan *et al.*, 2004; Singh *et al.*, 2006; for a review, see Burley & Bonanno, 2002). For future studies, we desire a robust method for the expression and isolation of mutant or full-length mitoNEET. Since the full-length protein includes a transmembrane helix, it may be more difficult to express and purify. Assessing the structural integrity of the fused constructs is also important for the interpretation of cellular localization experiments (Taminelli *et al.*, 2008; Lin *et al.*, 2007). As a first step, we constructed a fusion of the soluble domain of mitoNEET with the superfolder green fluorescent protein (sfGFP; Pedelacq *et al.*, 2005) designed to improve the expression of less soluble proteins. A thrombin cleavage site was engineered in between the proteins to facilitate the isolation of mitoNEET following expression of the sfGFP-mitoNEET fusion. We show that mitoNEET purified from the fusion protein contains the 2Fe–2S clusters and that the protein purified from the construct can be crystallized. We present the X-ray crystallographic structure of this mitoNEET (33–108) (PDB code 3ew0). Owing to the design of the construct, the extended N-terminus of the isolated mitoNEET was resolved. Upon comparison with other mitoNEET structures, we show that while the CDGSH domain is superimposable, the cytoplasmic tethering domain can be in multiple orientations, which could be functionally important.

2. Materials and methods

2.1. Fusion-construct cloning

The portion of the *CISD1* cDNA encoding the cytoplasmic part of the protein (residues 33–108) was subcloned into a modified pET28-a(+) vector (Novagen) that contained the sfGFP cDNA (Pedelacq *et al.*, 2006). MitoNEET was subcloned downstream of the superfolder cDNA using the *Bam*HI restriction site. A thrombin cleavage site and small linker were added upstream of the mitoNEET cDNA through PCR amplification of the mitoNEET cDNA using the forward primer 5′-GGCGGATCCTCTGGCCTCGTCCCTCGTGGCTCTGGCATGAGATTTTATG-3′ and the reverse primer 5′-GCCGCCGGATCCTTAAGTTTCTTTTTTCTTGATGATCAG-3′. The resulting construct was confirmed by sequencing.

2.2. Expression of the fusion protein, fusion cleavage and mitoNEET purification

Escherichia coli BL21-CodonPlus(DE3)-RIL cells were transformed with the sfGFP-mitoNEET cDNA construct and were grown in LB supplemented with 30 µg ml^{-1} kanamycin and 34 µg ml^{-1} chloramphenicol. Cells were grown and induced as described previously (Wiley, Paddock *et al.*, 2007). At an OD_{600} of 0.4, 0.75 m*M* $FeCl_3$ was added and cells were harvested by centrifugation after an additional 18–24 h of growth at 303 K. Cells were lysed by sonication. Ammonium sulfate was added to the lysate to 60% and the lysate was then pelleted by centrifugation. The pellet was solubilized in approximately 50–100 ml cleavage buffer (50 m*M* Tris–HCl pH 8.0, 100 m*M* NaCl, 2 m*M* $CaCl_2$) and thrombin (3 mg ml^{-1}) was added to a final concentration of 0.1 mg ml^{-1}. This solution was dialyzed at 277 K overnight against 4 l of the cleavage buffer with one change. After 24 h, a sample of the dialysate was run on an SDS–PAGE gel to ensure >90% thrombin cleavage efficiency. The thrombin inhibitor PPAC was added to the dialysate, which was then dialyzed against 4 l 50 m*M* Tris–HCl pH 8.0 for an additional 16 h at 277 K. To separate mitoNEET from sfGFP and other contaminating proteins, the solution was loaded onto a 5 ml cation-exchange column (S HP Hi-Trap, GE Healthcare) and mitoNEET was purified as described previously (Paddock *et al.*, 2007). The mitoNEET fractions were further purified on a 30 × 2 cm S-100 size-exclusion column (GE Healthcare) equilibrated with 50 m*M* Tris–HCl pH 8.0 and 100 m*M* NaCl. The mitoNEET fractions from the size-exclusion chromatography were pooled and concentrated to 10 mg ml^{-1}. The protein purity was assessed to be >99% using SDS–PAGE and an A_{278}/A_{458} optical ratio of <2.3. The protein concentrations were determined by UV absorbance spectroscopy using ε_{278} = 9.13 mM^{-1} cm^{-1}.

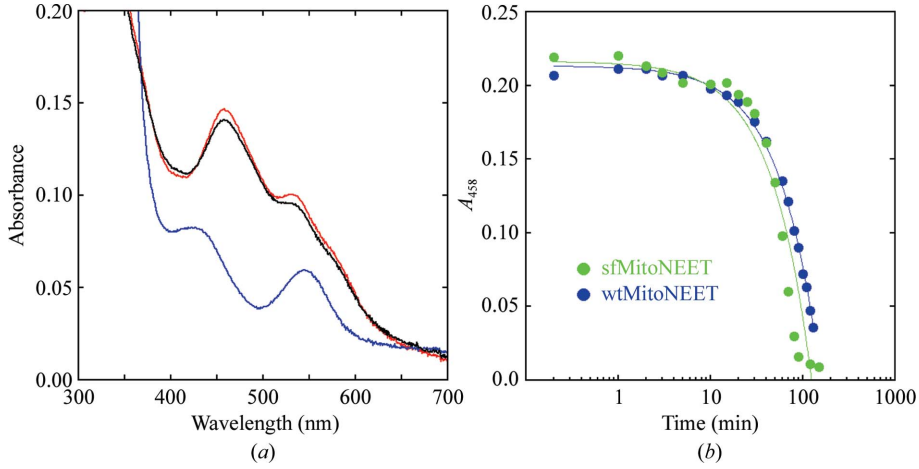

Figure 1
UV–visible spectra of the 2Fe–2S cluster of mitoNEET. (*a*) Absorption spectra of mitoNEET (33–108) purified from fusion protein recorded from 300 to 700 nm (red spectrum). Upon reduction by the addition of sodium dithionite (blue spectrum), the typical A_{458} peak is greatly reduced. Re-oxidation of the 2Fe–2S cluster occurs upon exposure to oxygen and is indicated by restoration of the typical A_{458} peak (black spectrum). This is identical to the behavior of the 2Fe–2S cluster in mitoNEET described previously (Paddock *et al.*, 2007; Wiley, Paddock *et al.*, 2007). (*b*) Time-dependent decay of the 2Fe–2S cluster at pH 6. MitoNEET purified from the sfGFP fusion (sfMitoNEET; green) is overlaid with wild-type mitoNEET purified without fusion (wtMitoNEET; blue). Results are consistent with those previously reported (Paddock *et al.*, 2007; Wiley, Paddock *et al.*, 2007).

2.3. UV–visible absorption spectroscopy

All UV–visible absorption spectra were measured from the near-UV to the near-IR (250–700 nm) on a Cary50 spectrometer (10–20 μ*M* protein in 50 m*M* Tris–HCl pH 8.0 and 50 m*M* NaCl) as described by Paddock *et al.* (2007). Chemical reduction of mitoNEET was achieved by adding dithionite to a final concentration of 2 m*M* at 295 K. Re-oxidation was achieved by equilibrating with ambient O_2 for 1 h.

2.4. Crystallization of mitoNEET purified from sfGFP fusion protein

Crystallization was achieved as described for mitoNEET (Paddock *et al.*, 2007). The final conditions were 100 m*M* Tris–HCl pH 8.0, 100 m*M* NaCl and 16–18% PEG 3000 in the protein well equilibrated against 100 m*M* Tris–HCl pH 8.0, 100 m*M* NaCl and 30–32% PEG 3000 in the reservoir. Crystals were frozen (77 K) after a 1 min soak in 100 m*M* Tris–HCl pH 8.0, 40% PEG 3000 and sent frozen (77 K) to SSRL in an SSRL-supplied cassette system for X-ray data collection and analysis.

2.5. X-ray data collection and refinement

Data were collected from cryogenically cooled crystals (100 K) on beamline 12.3.1 at the Advanced Light Source at Lawrence Berkeley National Laboratory using an X-ray wavelength of 1.158 Å and an oscillation angle of 1°. Data were collected from a single crystal and were processed to a high-resolution limit of 1.4 Å using an automated script developed by Qingping Xu at the Joint Center for Structural Genomics (JCSG, SSRL) that runs *XDS* (Kabsch, 1993). Although the unit-cell parameters of the mitoNEET crystals purified from the GFP-fusion expression vector are similar to those described by Paddock *et al.* (2007), preliminary analysis of the X-ray diffraction data indicated that the positioning of the subunits in the respective crystals were different. Therefore, molecular replacement was implemented for primary phasing with the program *Phaser* using the atomic coordinates of PDB entry 2qh7 as a search model. Model completion and refinement were performed in *Coot* (Emsley & Cowtan, 2004) and *REFMAC*5 (Winn *et al.*, 2003), respectively. Analyses of the stereochemical quality of the models were accomplished using an automated validation server developed by Chris Rife at the JCSG (SSRL) implementing *MolProbity* (Lovell *et al.*, 2003), *ADIT* (Yang *et al.*, 2004) and *WHATIF* 5.0.

3. Results and discussion

MitoNEET is easily overexpressed in large quantities as an sfGFP-mitoNEET fusion protein. To our knowledge, this is the first use of superfolder GFP as a fusion construct for Fe–S proteins; therefore our structural characterizations of mitoNEET purified from the GFP fusion construct were quite rigorous. UV–visible spectra (Fig. 1) and the structure determined from X-ray data (Figs. 2, 3 and 4) indicate that the mitoNEET obtained from the fusion construct maintains the properties of the native soluble mitoNEET.

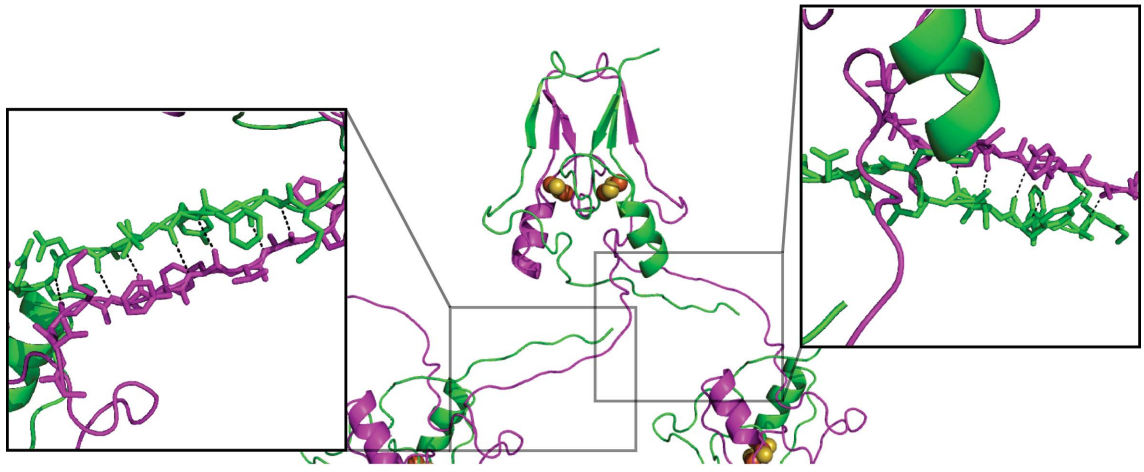

(*a*)

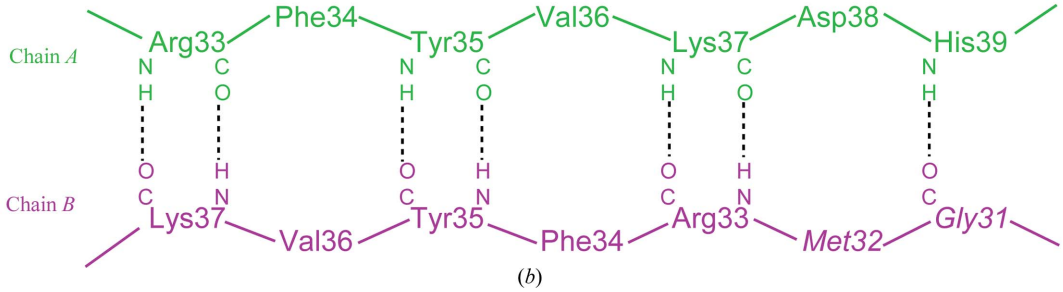

(*b*)

Figure 2
N-terminal crystal-packing interactions of mitoNEET purified from the sfGFP-mitoNEET fusion construct. (*a*) The crystal structure of mitoNEET purified from the sfGFP-fusion construct and part of two symmetry-related molecules (center panel) that interact through the N-termini (right and left boxes). The structure of mitoNEET was determined to 1.4 Å resolution. The 2Fe–2S centers are shown as atomic spheres (Fe in red and S in yellow). As with other mitoNEET structures, the two 2Fe–2S domains are within 16 Å (center to center) and are related by a dyad axis. In contrast to previous structures, the extended N-termini induced novel crystal contacts within the crystal. These interactions each involve seven backbone hydrogen bonds (see boxes) that are unique to each terminus of the two protomers. (*b*) The amino-acid residues in the N-terminal regions that interact through backbone hydrogen bonds (dotted lines) in the crystal structure. The different conformations of the two N-termini result from a 'register' shift of the backbone interactions from Arg33 through His39 in chain *A* and Gly31 through Lys37 in chain *B*.

3.1. UV–visible spectroscopic properties of mitoNEET

The 2Fe–2S centers of mitoNEET have characteristic absorption maxima at 458 and 530 nm (Wiley, Paddock *et al.*, 2007), similar to but distinct from other protein-bound Fe–S centers. MitoNEET purified and isolated from the sfGFP fusion shows the same characteristic absorbance peaks (Fig. 1*a*, red spectrum). After reduction, the A_{458} peak is largely diminished (Fig. 1*a*, blue spectra). The time-dependent decay of the A_{458} signal indicating the loss of 2Fe–2S upon adjusting the pH to 6.0 is shown in Fig. 1(*b*) and is within error of that previously described (blue; Paddock *et al.*, 2007; Wiley, Paddock *et al.*, 2007). The observed absorption characteristics of the purified protein indicate that despite being obtained from a fusion the 2Fe–2S clusters have retained all of their UV–visible spectroscopic characteristics.

3.2. Crystal structure of mitoNEET obtained from the fusion construct

Crystals of mitoNEET purified from the sfGFP-mitoNEET protein were grown as described by Paddock *et al.* (2007). The protein crystallized in the same space group as the native, $P2_12_12_1$, with slightly different unit-cell parameters: $a = 50.74$, $b = 48.48$, $c = 59.25$ Å. The structure was solved at 1.4 Å resolution (91.3% completeness) with an R factor of 20.2% ($R_{\rm free}$ = 24.4%).

The refined model reveals a homodimeric structure that is tightly packed, with ∼2000 Å^2 of buried surface area at the interface (Fig. 2, middle). Each protomer is composed of the following secondary-structural elements: an antiparallel β-structure, a swapping β-strand, an α-helix, a helical turn and 11 interconnecting β-turns. The homodimer is folded into two distinct domains. One domain is composed of a β-cap sandwich that includes the β-strand swap (Fig. 2). These two strand-swapped sheets pack together to form the β-cap sandwich domain and the narrowest part (∼15 Å across) of the structure. The swapped regions come from opposite ends of the primary sequence. The second domain, the cluster-binding domain, is larger (∼30 Å across) and contains the single helix from each protomer. It also harbors the two 2Fe–2S clusters, which are separated by approximately 16 Å (center to center) from each other. Each 2Fe–2S center is coordinated by three Cys residues and one His residue, resulting in the unique UV–Vis spectra (Fig. 1).

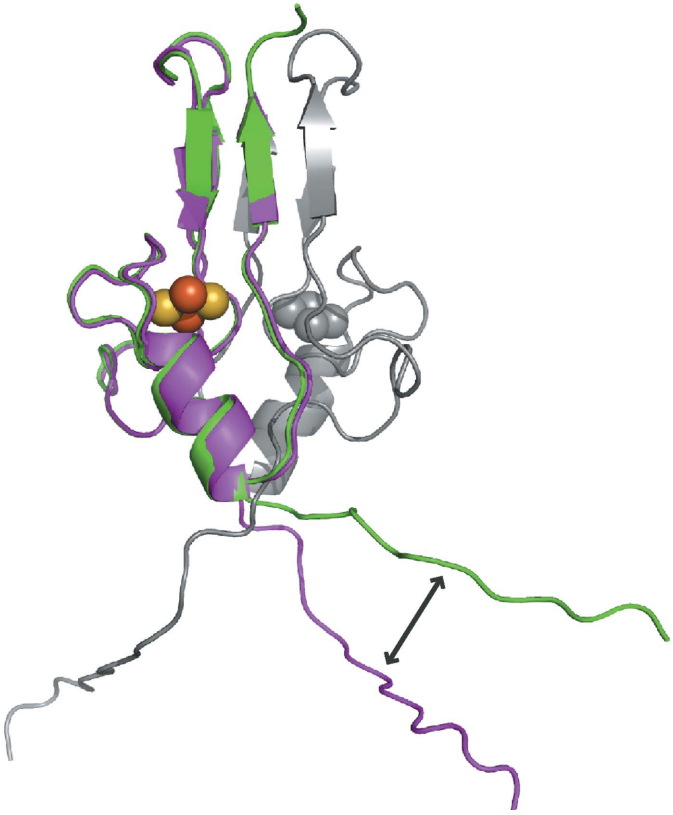

Figure 3
Flexibility of the N-termini in the crystal structure. Shown is a superposition of protomer *B* (green) onto protomer *A* (magenta). The original position of protomer *B* is shown in gray. Although the majority of the soluble domain is nearly identical, resulting in an internal dyad axis, the N-termini break the dyad axis of the homodimer. The arrow indicates differences in the directions of the N-termini.

Table 1
Summary of crystal parameters, data-collection and refinement statistics for mitoNEET purified from an sfGFP fusion.

Values in parentheses are for the highest resolution shell.

Space group	$P2_12_12_1$
Unit-cell parameters (Å, °)	a = 50.74, b = 48.48, c = 59.25, α = 90.00, β = 90.00, γ = 90.00
Data collection	λ_1, native
Wavelength (Å)	1.1158
Resolution range (Å)	38.5–1.40
No. of observations	169484
No. of unique reflections	26874
Completeness (%)	91.1 (76.3)
Mean $I/\sigma(I)$	19.60 (4.3)
$R_{\rm merge}$ on I† (%)	5.9 (32.7)
Model and refinement statistics	
Data set used	λ_1
Cutoff criterion	$\|F\| > 0$
Resolution range (Å)	38.5–1.40
No. of reflections (total)	26847‡
No. of reflections (test set)	1371
Completeness (%)	91.3
$R_{\rm cryst}$§	0.202
$R_{\rm free}$¶	0.244
Stereochemical parameters	
Restraints (r.m.s. observed)	
Bond angle (°)	1.66
Bond length (Å)	0.012
Average isotropic B value (Å^2)	5.64
ESU†† based on $R_{\rm free}$ (Å)	0.078

† $R_{\rm merge} = \sum_{hkl}\sum_i |I_i(hkl) - \langle I(hkl)\rangle| / \sum_{hkl}\sum_i I_i(hkl)$, where $I_i(hkl)$ is the scaled intensity of the ith measurement and $\langle I(hkl)\rangle$ is the mean intensity for that reflection. ‡ Typically, the number of unique reflections used in refinement is slightly lower than the total number that were integrated and scaled. Reflections are excluded owing to systematic absences, negative intensities and rounding errors in the resolution limits and unit-cell parameters. § $R_{\rm cryst} = \sum_{hkl} ||F_{\rm obs}| - |F_{\rm calc}|| / \sum_{hkl} |F_{\rm obs}|$, where $F_{\rm calc}$ and $F_{\rm obs}$ are the calculated and observed structure-factor amplitudes, respectively. ¶ $R_{\rm free}$ is as for $R_{\rm cryst}$, but calculated using 5% of the total reflections chosen at random that were omitted from refinement. †† ESU, estimated overall coordinate error.

3.3. N-terminal crystal-packing interactions of mitoNEET isolated from the sfGFP-fused construct

The extended N-termini of mitoNEET isolated from the fused construct were resolved in the crystal structure (Fig. 2). The N-terminus of one protomer interacts with the N-terminus of a symmetry-related molecule through seven backbone hydrogen bonds. Although both N-termini are resolved, they have distinct inter-protein interactions that result in different conformations in the crystal (left and right panels of Fig. 2*a*). This is also illustrated in Fig. 3, in which protomer *B* (green) was superimposed onto protomer *A* (magenta). The majority of the soluble protein, which includes the 2Fe–2S cluster-binding domains and the upper β-cap domains, displayed no differences outside of the intrinsic error of the structural model. This symmetry results in an internal dyad axis within the homodimer as previously reported (Paddock *et al.*, 2007; Lin *et al.*, 2007; Hou *et al.*, 2007). However, the resolved N-termini break the dyad axis (Fig. 3) owing to their unique interactions with symmetry-

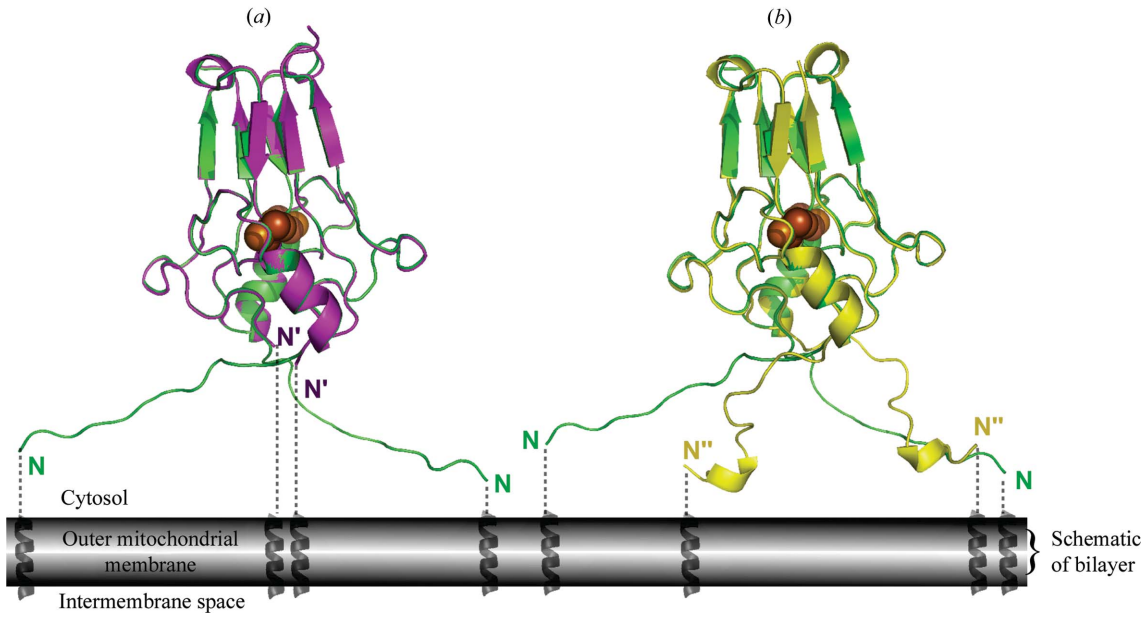

Figure 4
Structural comparison of mitoNEET purified from the sfGFP-fusion protein with mitoNEET isolated from nonfused constructs. (*a*) The newly obtained structure (colored green) is superimposed on the previously determined mitoNEET structure (magenta; Paddock *et al.*, 2007; PDB code 2qh7); the 2Fe–2S centers were used for the superposition. Note that the cluster-binding domains and the β-cap domains of the two structures are superimposable. (*b*) The new structure (green) superimposed on 2r13 (yellow; Hou *et al.*, 2007), the nonfused construct with well resolved N-termini. The two N-termini of the current structure differ both from each other and from the orientations resolved in a previous structure.

related molecules (Fig. 2). The different conformations of the two N-termini result from a 'register' shift of the N-terminal backbone hydrogen-bond interactions that are all within 3.0 Å. Chain *A* interacts from the backbone N atom of Arg33 through the backbone N atom of His39 with the backbone carbonyl of Gly31 through the backbone carbonyl of Lys37 of chain *B* as shown in Fig. 2 (bottom). Thus, the N-termini have sufficient flexibility to allow the alternate conformations observed in the crystal structure.

3.4. Comparison with nonfused mitoNEET structures

The cluster-binding and β-cap regions corresponding to amino acids 43–106 of mitoNEET are nearly identical within error to the previously published structures (Hou *et al.*, 2007; Lin *et al.*, 2007; Paddock *et al.*, 2007; Fig. 4). This shows that mitoNEET isolated from the sfGFP fusion construct is properly assembled. In addition, the N-terminal residues 32–42 were resolved in the current structure (Fig. 4*a*, green); they could not be seen in two of the previously published structures (Fig. 4*a*, magenta) (Lin *et al.*, 2007; Paddock *et al.*, 2007). In one of the previously published structures (Hou *et al.*, 2007) the N-termini were resolved (Fig. 4*b*, yellow), but the structure of the arms differed greatly from those found in the current structure (Fig. 4, green), despite similar cluster-binding and β-cap regions. Hence, while the structural domains of mitoNEET are organized, there appears to be a lot of flexibility in the N-terminal portion of the protein. This flexibility in the cytoplasmic tethering domain may be important for proper mitoNEET function. The ability of the soluble domain to move freely owing to N-terminal flexibility may be required for successful partner-protein interactions.

This work was supported by NIH grants GM41637 (to MO and MLP), GM54038 and DK54441 (to PAJ). RN thanks the Zevi Hermann Shapira Foundation for supporting the collaborative USA–Israeli efforts and George Feher, Mel Okamura and Don Blumenthal for many helpful discussions and enthusiastic support. Portions of this research were carried out at the Stanford Synchrotron Radiation Laboratory, a national user facility operated by Stanford University on behalf of the US Department of Energy, Office of Basic Energy Sciences. The SSRL Structural Molecular Biology Program is supported by the Department of Energy, the Office of Biological and Environmental Research, the National Institutes of Health, National Center for Research Resources, the Biomedical Technology Program and the National Institute of General Medical Sciences. The X-ray data collection was performed in Berkeley. The X-ray scattering and diffraction technologies and their applications to the determination of macromolecular shapes and conformations at the SIBYLS beamline at the Advanced Light Source, Lawrence Berkeley National Laboratory were supported in part by the DOE program Integrated Diffraction Analysis Technologies (IDAT) and the DOE program Molecular Assemblies Genes and Genomics Integrated Efficiently (MAGGIE) under Contract No. DE-AC02-05CH11231 with the US Department of Energy. Efforts to apply SAXS and crystallography to characterize eukaryotic pathways relevant to human cancers were supported in part by National Cancer Institute grant CA92584.

References

Burley, S. K. & Bonanno, J. B. (2002). *Annu. Rev. Genomics Hum. Genet.* **3**, 243–262.
Colca, J. R., McDonald, W. G., Waldon, D. J., Leone, J. W., Lull, J. M., Bannow, C. A., Lund, E. T. & Mathews, W. R. (2004). *Am. J. Physiol. Endocrinol. Metab.* **286**, E252–E260.
Emsley, P. & Cowtan, K. (2004). *Acta Cryst.* D**60**, 2126–2132.
Hou, X., Liu, R., Ross, S., Smart, E. J., Zhu, H. & Gong, W. (2007). *J. Biol. Chem.* **282**, 33242–33246.
Juan, H.-F., Liu, H.-L. & Hsu, J. P. (2004). *Curr. Proteomics*, **1**, 183–197.
Kabsch, W. (1993). *J. Appl. Cryst.* **26**, 795–800.

Lin, J., Zhou, T., Ye, K. & Wang, J. (2007). *Proc. Natl Acad. Sci. USA*, **104**, 14640–14645.
Lovell, S. C., Davis, I. W., Arendall, W. B. III, de Bakker, P. I., Word, J. M., Prisant, M. G., Richardson, J. S. & Richardson, D. C. (2003). *Proteins*, **50**, 437–450.
Lowell, B. B. & Shulman, G. I. (2005). *Science*, **307**, 384–387.
Meyer, J. (2008). *J. Biol. Inorg. Chem.* **13**, 157–170.
Paddock, M. L., Wiley, S. E., Axelrod, H. L., Cohen, A. E., Roy, M., Abresch, E. C., Capraro, D., Murphy, A. N., Nechushtai, R., Dixon, J. E. & Jennings, P. A. (2007). *Proc. Natl Acad. Sci. USA*, **104**, 14342–14347.
Pedelacq, J. D., Cabantous, S., Tran, T., Terwilliger, T. C. & Waldo, G. S. (2006). *Nature Biotechnol.* **24**, 79–88.
Singh, S., Malik, B. K. & Sharma, D. K. (2006). *Bioinformation*, **1**, 314–320.
Skov, V., Glintborg, D., Knudsen, S., Tan, Q., Jensen, T., Kruse, T. A., Beck-Nielsen, H. & Hojlund, K. (2008). *PLoS ONE*, **3**, e2466.
Taminelli, G. L., Sotomayor, V., Valdivieso, A. G., Teiber, M. L., Marin, M. C. & Santa-Coloma, T. A. (2008). *Biochem. Biophys. Res. Commun.* **365**, 856–862.
Wiley, S. E., Murphy, A. N., Ross, S. A., van der Geer, P. & Dixon, J. E. (2007). *Proc. Natl Acad. Sci. USA*, **104**, 5318–5323.
Wiley, S. E., Paddock, M. L., Abresch, E. C., Gross, L., van der Geer, P., Nechushtai, R., Murphy, A. N., Jennings, P. A. & Dixon, J. E. (2007). *J. Biol. Chem.* **282**, 23745–23749.
Winn, M. D., Murshudov, G. N. & Papiz, M. Z. (2003). *Methods Enzymol.* **374**, 300–321.
Yang, H., Guranovic, V., Dutta, S., Feng, Z., Berman, H. M. & Westbrook, J. D. (2004). *Acta Cryst.* D**60**, 1833–1839.